Front. Earth Sci. 2024, 18(4): 849−863
https://doi.org/10.1007/s11707-022-1032-z

RESEARCH ARTICLE

Projected changes of runoff in the Upper Yellow River Basin under shared socioeconomic pathways

Ziyan CHEN[1], Buda SU (✉)[1], Mengxia ZHAO[2], Yim ling SIU[4], Jinlong HUANG[1], Mingjin ZHAN[3], Tong JIANG (✉)[1]

1 Collaborative Innovation Center on Forecast and Evaluation of Meteorological Disasters/Institute for Disaster Risk Management /School of Geographical Science, Nanjing University of Information Science & Technology, Nanjing 210044, China
2 Academy of Disaster Reduction and Emergency Management (Ministry of Emergency Management and Ministry of Education), Beijing Normal University, Beijing 100875, China
3 Jiangxi Eco-meteorological Center, Nanchang 330000, China
4 Sustainability Research Institute, School of Earth & Environment, University of Leeds, Leeds LS2 9JT, UK

Abstract Climate change has significantly impacted the water resources and conservation area of the Yellow River basin. The Upper Yellow River basin (UYR), referring to the area above Lanzhou station on the Yellow River is the focus of this study, the runoff changes in the UYR would greatly impact the water resources in China. Most existing studies rely on a single hydrological model (HM) to evaluate runoff changes instead of multiple models and criteria. In terms of the UYR, outputs of the previous Coupled Model International Comparison Project (CMIP) are used as drivers of HMs. In this study, the weighted results of three HMs were evaluated using multiple criteria to investigate the projected changes in discharge in the UYR using the Shared Socioeconomic Pathways (SSPs) from CMIP6. The research's key findings include the following. 1) Annual discharge in the UYR is expected to increase by 15.2%−64.4% at the end of the 21st century under the 7 SSPs. In the long-term (2081−2100), the summer and autumn discharge will increase by 18.9%−56.6% and 11.8%−70%, respectively. 2) The risk of flooding in the UYR is likely to increase in the three future periods (2021−2040, 2041−2060, 2081−2100) under all 7 SSPs. Furthermore, the drought risk will decrease under most scenarios in all three future periods. The verified HMs and the latest SSPs are applied in this study to provide basin-scale climate impact projections for the UYR to support water resource management.

Keywords Shared Socioeconomic Pathways (SSPs), climate change, discharge, the Upper Yellow River basin

Received November 16, 2021; accepted October 9, 2022

E-mails: subd@nuist.edu.cn (Buda SU)
jiangtong@nuist.edu.cn (Tong JIANG)

1 Introduction

Global warming will lead to the acceleration of the regional hydrological cycle, which in turn will impact regional water resources, river runoff, and terrestrial ecology (Su et al., 2017; Gao et al., 2019; Zhao et al., 2020; Qin et al., 2021). In comparison with before industrialization, the temperature of the global surface had increased by 1.05 [0.95−1.20] °C in 2011−2020, and 2015−2020 were the hottest 5 years on record (IPCC, 2021; Sun, 2021). As far as the global land area is concerned, there is no obvious trend in precipitation, but regional precipitation has changed in the mid-latitude region in the Northern Hemisphere since 2000 (Stocker et al., 2014). Scientific projection of river runoff under a warming climate is the basis for water resource utilization and management and has important significance for flood control, drought relief, and disaster reduction (Wang et al., 2018)

The Upper Yellow River basin (UYR) in China is very sensitive to climate change (IPCC, 2001; Wang et al., 2018; Li et al., 2022). The UYR makes up 28.8% of the catchment area of the Yellow River basin, and is a significant water replenishment area and conservation area for the entire river basin (Meng et al., 2016; Wei et al., 2021). There are many reservoirs in the UYR, but high variability in runoff and precipitation poses a challenge to reservoir operation and management. Climate and runoff changes in the UYR under changing conditions have significant implications for reducing soil erosion, preventing droughts and floods, and ensuring the implementation of the national strategy of "regional ecological protection and high-quality development" (Zuo, 2019).

Hydrological models (HMs) are vitally important tools for studying the effect of climate variation on river runoff. The accuracy of hydrological modeling in watersheds is vital to reduce the uncertainty in climate change impact assessments. Most existing studies rely on a single HM and several hydrological criteria to evaluate runoff changes (Huang, 2014; Höllermann and Evers, 2017; Qin et al., 2019; Chen et al., 2020; Zhao et al., 2020). However, compared with a single HM, the result of the multi-HM simulation is more in line with the actual conditions of a basin. The most commonly used multi-HM simulation is based on the arithmetic mean or median (Vetter et al., 2015; Su et al., 2017; Gao et al., 2019) and simply ignores the differences among HM performances. Some scholars suggest assigning different weights to HMs to reduce the model-related uncertainty in the climate impact assessment by utilizing a comprehensive assessment method (Shamseldin et al., 2007; Arsenault et al., 2015). Furthermore, the performances of HMs should be evaluated at different river sections in the basin, not only at the outlet (Krysanova et al., 2018). Several studies are calibrating and verifying HMs by multisite, multivariable, and multistandard simulations, and achieving remarkable results (Eghdamirad et al., 2019; Puertes et al., 2019; Wen et al., 2020). Therefore, multisite, multivariable, and multistandard simulations are used in this study to calibrate and verify HMs in UYR.

As a driver of HMs, climate scenarios exert a principal role in investigating the effect of climate change on river basin runoff. In the past 30 years, climate models have made considerable progress (Lambert and Boer, 2001; Torres and Marengo, 2014; Huang et al., 2018; Gao et al., 2019). The Coupled Model International Comparison Project (CMIP) has constructed the most extensive climate model database to date (Zhou et al., 2019). It provides an irreplaceable scientific basis for the projection of climate change, including comprehensive overviews of possible changes in future climate under different designed emission scenarios by the assessment report series of the Intergovernmental Panel on Climate Change (IPCC) (Vuuren et al., 2011; Taylor et al., 2012). CMIP6 combines previous Shared Socioeconomic Pathways (containing SSP1: Sustainability; SSP2: Middle of the Road; SSP3: Regional Rivalry; SSP4: Inequality; SSP5) with Representative Concentration Pathways (RCPs) to form new SSPs (containing SSP1-1.9, SSP1-2.6, and SSP2-4.5, SSP3-7.0, SSP4-3.4, SSP4-6.0 as well as SSP5-8.5) (O'Neill et al., 2016). Not only the possible social and economic development scenarios are considered, but also the changes in future radiation forcing from low to high are covered by the latest SSPs. It is an ideal choice for climate change-related research (Gidden et al., 2019) General Circulation Model (GCM), the output content of different stages of CMIPs has long been the core of climate change research. Now, previous studies on runoff in the UYR were principally determined by the outputs of CMIP3 together with CMIP5 (Kang et al., 2015; Chen, 2017; Yan, 2017; Zhou et al., 2019). The results show that relative to the 1971–2000 period, as of the mid-21st century, runoff is expected to increase by approximately 2.7%–17% under the representative concentration pathways (RCPs), which describe different trajectories for carbon dioxide emissions.

Intending to ensure that climate impact investigations meet the requirements of stakeholders for reliable information at the regional level, verified HMs and the latest SSPs should be used to provide basin-scale climate impact projections (Vetter et al., 2015). However, to date, no similar research has been conducted in the UYR. Therefore, we have conducted a comprehensive assessment of the Soil Water Assessment Tool (SWAT) (Arnold et al., 1998), Hydrologiska Byråns Vattenbalansavdelning model (HBV) (Bergström and Forsman, 1973; Krysanova et al., 1999), and Variable Infiltration Capacity model (VIC) (Xu et al., 1994) based on observed data in the UYR to parameterize HMs, and subsequently, HMs are further driven by the five climate models from the latest CMIP6 to simulate future discharge to study the climate change impacts on annual, seasonal, and extreme discharge under SSPs. This study is expected to compensate for the discharge simulation with verified HMs and CMIP6 projection under the latest SSPs in the context of climate change in the UYR. Other comparable studies in various basins with similar climatic and hydrological conditions can take this study as a reference.

2 Study area and data

2.1 Study area

The area located in the UYR above the Lanzhou Hydrological Station (32.4°–41.8°N, 95.8°–112.0°E), which includes a watershed area of 21.6×10^4 km^2, is selected in this study. It accounts for approximately 28% of the whole Yellow River basin and provides 54% of the river runoff at the outlet of the Yellow River basin. With abundant streamflow, the UYR represents a source of clear water and the main water storage area of the Yellow River (Chang et al., 2017; Zhou et al., 2019). The Ji Mai, Ma Qu, Tang Naihai, and Lan Zhou hydrological stations represent basin areas of approximately 4.5×10^4 km^2, 8.6×10^4 km^2, 12.2×10^4 km^2, and 21.6×10^4 km^2, respectively, in the UYR (Fig. 1).

Most of the UYR is located in arid and semiarid regions, with complex topography ranging from 1514 to 6217 m. The annual mean temperature can reach 3.98°C, while the annual precipitation is approximately 461.9 mm in the UYR (1961–2018). The climate in the UYR is affected by the south-west monsoon, south-east monsoon, and Qinghai-Xizang Plateau and is sensitive to climate

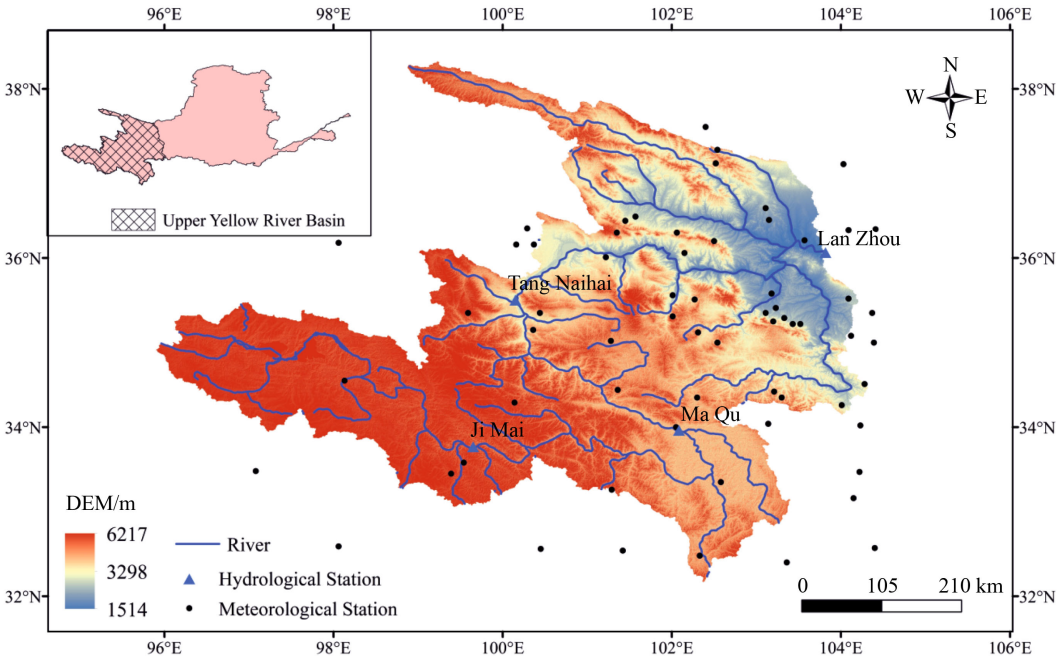

Fig. 1 Location of 4 hydrological stations and 53 meteorological stations in the Upper Yellow River basin.

change. The flood season is from May to September, and rainfall during the flood season accounts for approximately 82% of the annual total. The UYR is of strategic significance for the sustainable development of the Yellow River basin and China as a whole.

2.2 Data

2.2.1 Observed data

The Observed daily meteorological data observed at 53 ground-based stations from 1961 to 2014 in the UYR, which are quality controlled by considering changes in instruments and locations, are offered by the National Meteorological Information Centre of China Meteorological Administration.

The daily discharge data for the period 1961−2014 at the Lan Zhou, Tang Naihai, Ma Qu, and Ji Mai stations were obtained from the China Hydrological Yearbook-Yellow River. Data between 1962 and 1968, when human influences on river runoff were comparatively less, were utilized for calibrating and validating three selected HMs (i.e., SWAT, HBV-D, and VIC).

The digital elevation model (DEM) used in this study is 90 m resolution from the Shuttle Radar Topography Mission (SRTM) and was produced by processing radar images. The data of land use (where the resolution is 1 km) are acquired from the Resources and Environmental Science Data Center, Chinese Academy of Sciences, Soil data with a resolution of 1 km were taken from the Harmonized World Soil Database (HWSD), which was established through the Food and Agriculture Organization (FAO) of the United Nations and the International Institute for Applied Systems in Vienna (IIASA) and adopted the FAO-90 soil classification system.

2.2.2 Climate model data

Climate change characteristics for historical and future periods were analyzed in the UYR by using 5 GCM outputs from the latest CMIP6. For these data, average temperature, daily precipitation, minimum and maximum temperature covering the historical period (from 1995 to 2014) along with future period (from 2015 to 2100) under all seven SSPs were collected. At the time of this writing, all variables required by the seven SSPs were available from a total of 5 models, namely, IPSL-CM6A-LR, CNRM-ESM2-1, CanESM5, MRI-ESM2-0, and MIPOC6 (Table 1). In the current paper, the future climate variation in the UYR and its impact on discharge are assessed in three time periods: from 2021 to 2040 (near-term), from 2041 to 2060 (medium-term), and from 2081 to 2100 (long-term) relative to the reference period (from 1995 to 2014). Due to the large differences in their resolutions, the GCM outputs were downscaled and bias corrected through inverse distance weighting (IDW) interpolation and equidistant cumulative distribution functions (EDCDF) methods (Franke, 1982; Li et al., 2010). For comparison purposes, the spatial resolution for all the output data of GCM had been downscaled to 0.5° × 0.5°.

The combination of climate policies and SSPs produces various outputs at the end of this century. The radiative force in 2100 is 1.9, 2.6, 3.4, 4.5, 6.0, 7.0, or 8.5 W each square meter (Vuuren et al., 2011; O'Neill et al., 2016;

Table 1 A brief overview of the 5 GCMs from CMIP6

Model name	Institution with country	Original horizontal resolution (Lon × Lat)	Resolution after downscaling (Lon × Lat)
CanESM5	Canadian Centre for Climate Modeling and Analysis, Environment and Climate Change, Canada	~2.8 × 2.8	0.5 × 0.5
CNRM-ESM2-1	Centre National de Recherches Meteorologiques- Centre Europeen de Recherche et de Formation Avancee en Calcul Scientifique (CNRM-CERFACS), France	2.5 × 1.2676	0.5 × 0.5
IPSL-CM6A-LR	Institut Pierre Simon Laplace, France	2.5 × 1.2676	0.5 × 0.5
MIROC6	Japan Agency for Marine-Earth Science and Technology, Japan	1.4063 × 1.4	0.5 × 0.5
MRI-ESM2-0	Meteorological Research Institute, Japan	~1.125 × 1.12	0.5 × 0.5

Hausfather and Peters, 2020). Among the 7 SSPs in CMIP6, SSP4-3.4, SSP1-2.6 along with SSP1-1.9 are low radiative forcing scenarios, SSP2-4.5 and SSP4-6.0 are the medium radiative forcing scenarios, SSP3-7.0 represents the medium and high end of future warming and emissions ("Possible futures"), while SSP5-8.5 is a high radiative forcing scenario, which is regarded as the highly unlikely approach and is wrongly assumed to be "business as usual" (Hausfather and Peters, 2020).

3 Methodologies

3.1 Hydrological models

Three HMs, namely, SWAT, HBV-D, and VIC, were applied to the simulation of daily discharge at the Lan Zhou, Tang Naihai, Ma Qu, and Ji Mai hydrological stations. The three HMs have been successfully applied to climate impact studies in many regions with different hydroclimatic statuses (Gao et al., 2019).

SWAT is a continuous-time semi-distributed process-based HM, which describes the main hydrological processes at the river basin scale. The following water balance equation is used in SWAT (Arnold et al., 1998):

$$SW_t = SW_0 + \sum_{i=1}^{t}(R_{\text{day}} - Q_{\text{surf}} - E_{\text{a}} - W_{\text{seep}} - Q_{\text{gw}}), \quad (1)$$

where all variables are in millimeters (mm), except that t represents time with the unit 'day'. SW_t means the final soil moisture. SW_0 is the initial soil moisture content on the day i. R_{day}, Q_{surf}, E_{a}, W_{seep}, Q_{gw} represent the precipitation, surface runoff, evapotranspiration, amount of water entering the vadose zone from the soil profile, and return runoff on the day i, respectively.

As a precipitation-runoff model, HBV-D describes the processes of runoff generation via simple and robust structures, which are mainly driven by topography and climate. The total water balance equation of HBV-D is as follows (Bergström and Forsman, 1973):

$$P - E - Q = \frac{\text{d}}{\text{d}t}[\text{SP} + \text{SM} + \text{UZ} + \text{LZ} + \text{lakes}], \quad (2)$$

where P means precipitation, E means evapotranspiration and Q means runoff. Respectively, SP, SM, UZ, LZ, and lakes represent snow cover, soil water content, surface underground aquifer, deep underground aquifer, and lake water volume.

VIC is a semi-distributed hydrological model for large-scale applications. The land surface processes are modeled at a grid of large cells, and statistical distribution functions are used to handle the heterogeneity of the sub-grid. Through variable infiltration curve, parameterization of sub-grid variability in soil moisture holding capacity and nonlinear base flow, the runoff processes are represented. The routing of water flow is performed after processes in grid cells are simulated.

The property of these HMs was tested by the processes of validation and calibration in the historical period utilizing the comprehensive model evaluation method (Krysanova et al., 2018; Wen et al., 2020), which includes the following steps.

1) The quality of the meteorological input data (including temperature and precipitation) is checked.

2) In the basin, four hydrological stations are calibrated and validated simultaneously to ensure the consistency of the internal nature of the basin. The performances of the 3 HMs in the historical period are evaluated according to the comparison of the simulation with observations. The closer the relationship between them is, the more acceptable the model parameterization results are.

3) The ratio of root mean square error to standard deviation of observation (RSR), the Kling-Gupta efficiency (KGE) as well as Nash-Sutcliffe efficiency (NSE) were used to evaluate the performances of the 3 HMs (i.e., goodness-of-fit criteria). RSR $\leqslant$ 0.6, KGE $\geqslant$ 0.7, and NSE $\geqslant$ 0.7, these values are regarded as key thresholds for 'good' property (Moriasi et al., 2007; Gupta et al., 2009; Ritter and Muñoz-Carpena, 2013; Gao et al., 2019).

3.2 Determination of weight of HMs

In the case of a large difference in the outputs of HMs, the weighting of HMs has the advantage of increasing the contribution of the models that have better performances than others (Dawson et al., 2012; Wang et al., 2016). The

weight assigned to each model can be determined by the following equation:

$$k = \mathrm{NSE} + \mathrm{KGE}, \tag{3}$$

$$k = \left(1 - \frac{\sum_{t=1}^{N}(Q_{s,t} - Q_{o,t})^2}{\sum_{t=1}^{N}(Q_{s,t} - \bar{Q}_o)^2} + 1 - \sqrt{(r-1)^2 + (\beta-1)^2 + (\gamma-1)^2}\right), \tag{4}$$

$$w_i = \frac{k_i^a}{\sum_{t=1}^{N}\left(k_i^a\right)} \ (i \in 1,2,3), \tag{5}$$

where N represents the number of HMs (N = 3); Q_o and Q_s, respectively denote the observed and simulated discharge; r represents the correlation coefficient between the measured discharge and simulated discharge; γ and β are the variability ratio and bias ratio; k represents the sum of NSE and KGE; α = 0,1,2,3,4; and w_i is the weight. In the calculation process, the artificial trial and error method is used to test the weight results. Through the test, it is determined that the simulation result is the best when α = 2, and these weights are used to project the future discharge change in the basin.

3.3 Trend detection method

The Mann-Kendall test is a nonparametric method often used for determining the trend and the importance of changes in climate and hydrological time series (Mann, 1945; Moran and Kendall, 1951; Hamed and Ramachandra Rao, 1998). This method is chosen in this study to detect the significance of the trends of temperature, precipitation, and discharge in the UYR. When $|Z| \geqslant$ 1.64 (1.96, 2.58), there is a significant trend at the 0.1 (0.05, 0.01) significance level.

A Taylor diagram (Taylor et al., 2001) can represent the ratio of the central root mean square error, standard deviation, and correlation coefficient R to assess the model simulation property. In a standardized Taylor diagram, the radial length from origin denotes the ratio of the model to the observed standard deviation: the closer the model is to 1, the better the simulation ability is. The root mean square error is represented by a semicircle with the observation point as the center, with the closer the mode point comes to the observational point, the smaller the gap is. The azimuthal position indicates the correlation coefficient, and the closer the mode point is to the observation point, the higher the correlation coefficient between them.

When the daily discharge series is arranged from large to small, Q10 and Q90 represent 10% and 90% of the daily average discharge sequence, respectively, and the discharge beyond this value reflects the high flow and low flow, respectively.

4 Results

4.1 Evaluation of climate and hydrological models

4.1.1 Performance of the climate models

Bias-corrected model results show that the annual precipitation in the UYR for 1995−2014 is 503.6 mm by the multimodel ensemble, slightly higher than the observed annual precipitation of 502.1 mm. Meanwhile, the observed and simulated annual mean temperatures respectively are −0.13°C and −0.56°C.

At the seasonal scale, the mean temperature by the multimodel ensemble mean is 0.47°C lower than the observations in spring, 0.38°C lower than those in summer, 0.39°C lower than those in autumn, and 0.3°C lower than those in winter. The GCMs also simulate the intra-annual distribution of precipitation quite well, with correlation coefficients between the observed and modeled precipitation of approximately 0.9 for each month between 1995 and 2014.

After bias correction, simulated temperature and precipitation match with observations better than the original model outputs (Fig. 2). It also can be seen that the correlation between the modeled temperature (precipitation) by the multimodel ensemble and the observations is much higher than that of a single climate model. According to the Taylor diagram, the ratio of the multimodel ensemble median of the temperature (precipitation) to the standard deviation of the observed is close to 1. The root mean square error between the multimodel ensemble median and the observed value is smaller than that between a single model and the observed value. In short, the multimodel ensemble median of monthly temperature (precipitation) is better than that of a single model simulation, with correlation coefficients above 0.9, root mean square errors less than 0.2 (0.4), and standard deviation ratios of approximately 1. Considering these three aspects, the multimodel ensemble median will be applied in this study to analyze the local climate change and climate change impacts.

4.1.2 Performance of the hydrological models

The SWAT, HBV-D, and VIC are calibrated and validated by using the observed data. Two large reservoirs, the Liujiaxia Reservoir and Longyangxia Reservoir, which together account for 97% of the regulating capacity in the UYR, started operation in 1969 and 1987, respectively (Peng et al., 2018; Jia et al., 2019). The period before 1970, which was less affected by human activities, is selected for this study to parameterize HMs, the 1962−1964 period is used as the calibration period, and the 1965−1968 period is used for model validation.

Comparisons between the simulated and observed daily discharge show that the HMs can well reflect the dynamic

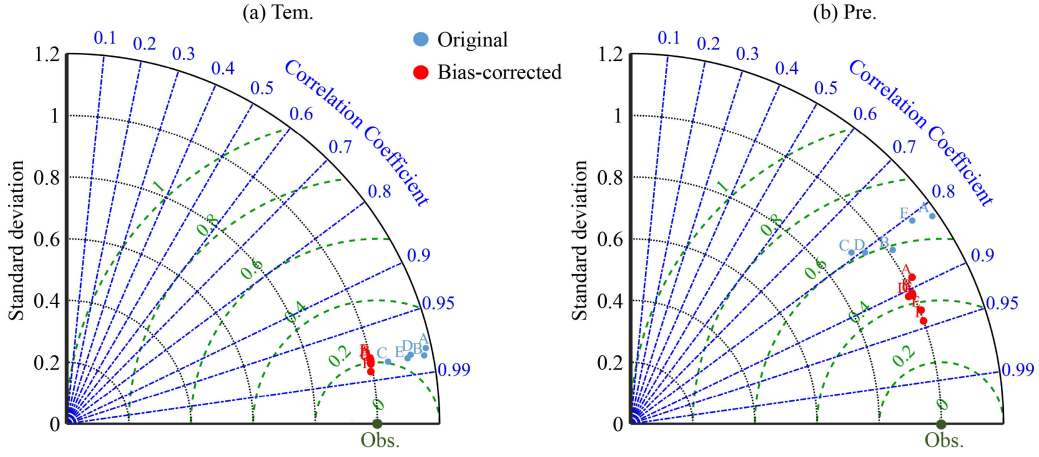

(A) CanESM5 (B) CNRM-ESM2-1 (C) MRI-ESM2-0 (D) IPSL-CM6A-LR (E) MIROC6 (F) Multi-model ensemble median

Fig. 2 Taylor diagram of CMIP6 modeled and observed temperature (a) and precipitation (b) in the Upper Yellow River basin.

changes in daily discharge at four stations. Among them, simulated discharge at the Lan Zhou, Tang Naihai, and Ma Qu hydrological stations is consistent with observations, and the NSE, KGE, and RSR values are 0.7−0.88, 0.70−0.89, and 0.35−0.53 in the course of validation and calibration. The property of SWAT was better than those of HBV-D and VIC at these three hydrological stations (Fig. 3 and Table 2).

However, it cannot be ignored that the HMs at the Ji Mai hydrological station in the headwater section have an average performance, with NSE values of 0.67−0.74, KGE values of 0.67−0.73, and RSR values of 0.5−0.63 in the calibration period and NSE values of 0.5−0.72, KGE values of > 0.7, and RSR values of < 0.7 in the validation period. The VIC model performed slightly better than the SWAT and HBV-D models. Previous studies have also shown that the simulation results of discharge in the headwaters of the Yellow River are poor, which might be related to complex snow and glacier melting processes (Xi et al., 2021). Although the simulation results at the Ji Mai station are of only average quality, the discharge passing the Ji Mai hydrological station accounts for only approximately 11% of the discharge passing the Lan Zhou hydrological station and has little influence on the simulation results by HMs in the UYR.

According to long-term mean monthly flow dynamics at the four hydrological stations, the observed and simulated discharge show good consistency in the process of validation and calibration (Fig. 4). The SWAT and HBV-D models slightly overestimated the discharge in the flood season (July to September), but the SWAT simulations in other months were the closest to the observed flow, while the VIC model underestimated the monthly discharge to a certain extent. From 1962 to 1968, the correlation coefficients between the simulated and observed discharge at the four hydrological stations

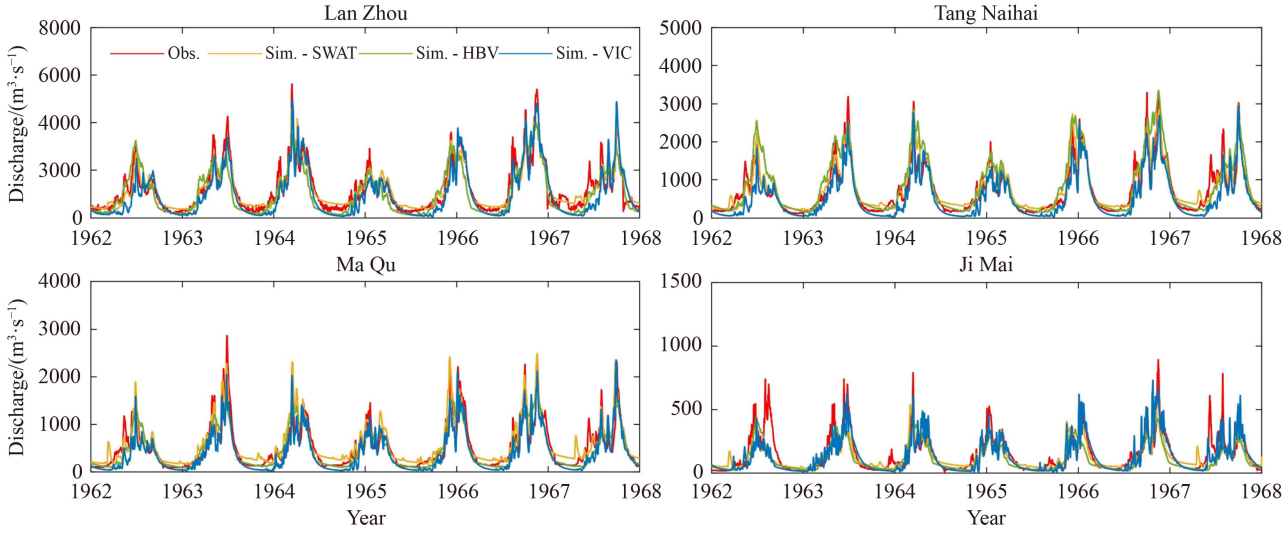

Fig. 3 Observed and simulated daily discharge through the three hydrological patterns (VIC, HBV-D, and SWAT) at the Lan Zhou, Tang Naihai, Ma Qu and, Ji Mai stations in the Upper Yellow River basin from 1962 to 1968.

Table 2 Evaluation of model property in the validation and calibration process in the Upper Yellow River basin, China

Criteria	Station	Calibration (1962−1964)			Validation (1965−1968)		
		SWAT	HBV-D	VIC	SWAT	HBV-D	VIC
NSE	Lan Zhou	0.87	0.76	0.76	0.84	0.76	0.75
	Tang Naihai	0.88	0.80	0.74	0.87	0.80	0.73
	Ma Qu	0.79	0.79	0.72	0.76	0.76	0.7
	Ji Mai	0.67	0.71	0.74	0.60	0.53	0.72
KGE	Lan Zhou	0.89	0.82	0.8	0.83	0.78	0.79
	Tang NaiHai	0.88	0.86	0.75	0.86	0.81	0.76
	Ma Qu	0.79	0.84	0.72	0.78	0.83	0.7
	Ji Mai	0.67	0.81	0.73	0.74	0.64	0.71
RSR	Lan Zhou	0.36	0.49	0.49	0.40	0.48	0.47
	Tang Naihai	0.35	0.45	0.51	0.35	0.45	0.45
	Ma Qu	0.46	0.46	0.53	0.49	0.48	0.47
	Ji Mai	0.63	0.53	0.5	0.57	0.68	0.53

Notes: NSE = the Nash-Sutcliffe efficiency; KGE = the Kling-Gupta efficiency; RSR represents the ratio of root mean square error to the observed standard deviation.

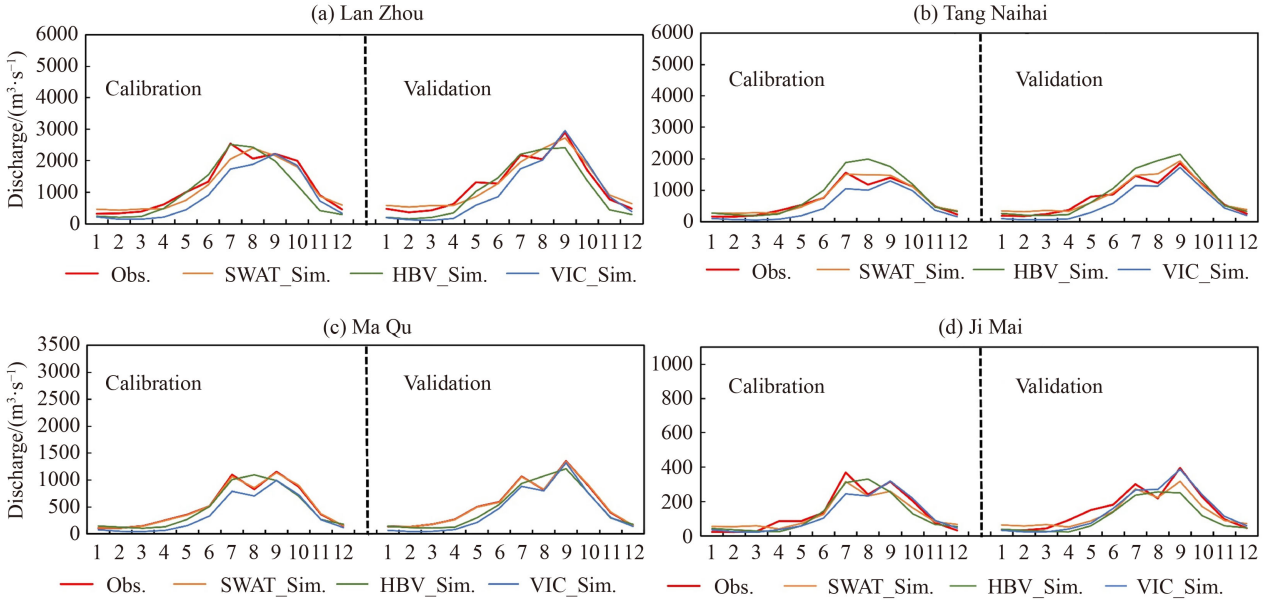

Fig. 4 Observed and simulated interannual discharge dynamics for 1962−1968 by the three HMs at the Lan Zhou, Tang Naihai, Ma Qu, and Ji Mai stations in the Upper Yellow River basin in China.

month by month were all above 0.82. In general, from the perspective of the distribution within the year and the correlation coefficient of discharge, the SWAT performances were better than those of HBV-D and VIC.

In addition, a comparison of the simulated annual Q10 and Q90 for 1962−1968 with those in the observed time series indicated that the Q10 (i.e., high flow) discharge simulated by the three HMs show good consistency with the observations, and their correlation coefficients are between 0.87 and 0.96. However, Q90 (i.e., low flow) is not simulated as well as Q10, with correlation coefficients of 0.52−0.66. For low flow values, the HBV-D model performs better than SWAT and VIC. SWAT overestimates Q90, while VIC underestimates Q90. In this case, it is necessary to apply weights to the HMs (Fig. 5).

Based on the performances of the HMs at multiple sites, it is clear that the three HMs can be used to simulate discharge in the UYR. In this study, the selected goodness-of-fit criteria are the most commonly used criteria for model evaluation, which can reflect the relationship between the simulated and observed discharge from many aspects. After a comprehensive evaluation of model performance, weights of 40%, 30%, and 30% are assigned to the SWAT, HBV-D, and VIC models, respectively, and as a result, a weighted daily discharge sequence can be obtained. The correlation

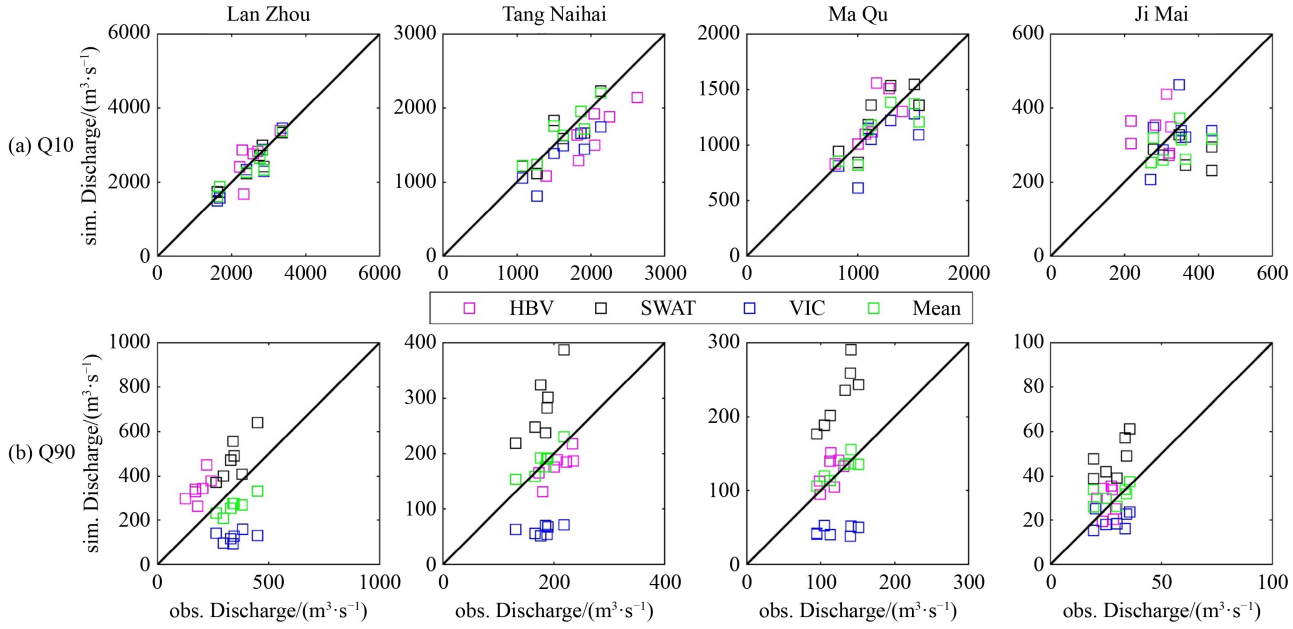

Fig. 5 Comparison of the Q10 (a) and Q90 (b) values simulated and observed at the Lan Zhou, Tang Naihai, Ma Qu, and Ji Mai stations in the Upper Yellow River basin during the calibration (1962−1964) and validation (1965−1968) periods.

coefficients between simulated and observed discharge at the four hydrological stations increase to more than 0.88 during 1962−1968. A comparison of the observed Q10 and Q90 with the weighted simulation results shows that the model simulation has improved significantly, which is reflected in the increase in the correlation coefficient between the simulation and observation and the decrease in the extreme deviation between the observation and simulation. At Lan Zhou station at the basin outlet, the deviation of observed and simulated Q10 shrinks from −5.1%–−1.6% to −2.1%, and the deviation of Q90 shrinks from −60.0%−39% to −16.8%. In addition, the correlation coefficient between the weighted month-by-month discharge and the simulated discharge is greater than 0.88, which exceeds the performance of a single model. In summary, weighting can improve the simulation results and reduce the uncertainty (Fig. 6).

4.2 Changes in temperature and precipitation in the 21st century

4.2.1 Annual mean temperature and annual precipitation

The widely used multimodel median technique is used to

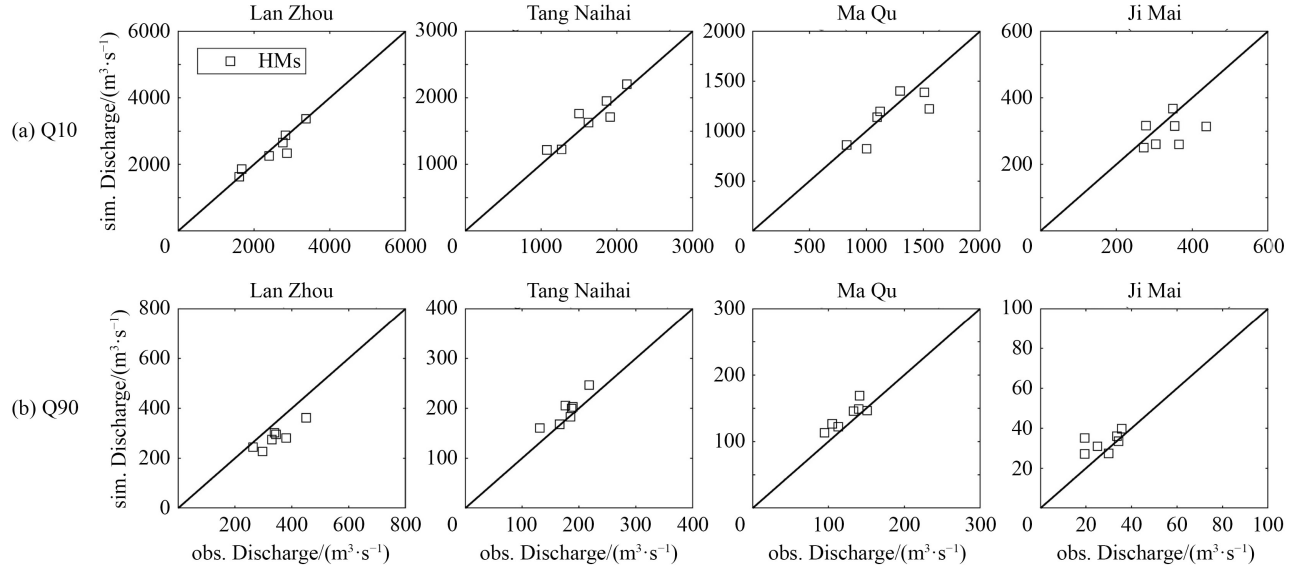

Fig. 6 Comparison of the Q10 (a) and Q90 (b) values simulated and observed at the Lan Zhou, Tang Naihai, Ma Qu, and Ji Mai hydrological stations in the Upper Yellow River basin for the validation (from 1965 to 1968) and calibration (from 1962 to 1964) process after weighting.

analyze the climate changes in the UYR under the seven SSPs in the three future periods (i.e., the near-, mid-, and long-term periods). Figure 7 shows that under all the SSPs in the 21st century, the annual precipitation and annual average temperature tend to increase, and the trends of warming and humidification become more significant at higher radiative forcings.

The UYR will experience warming throughout the 21st century under SSP1-2.6 and SSP1-1.9 (low-emission scenarios), with a growth rate of approximately 0.03°C/10yr−0.09°C/10yr. The increase rate of annual mean temperature will slow down during the mid-term period and then stabilize at 1.4°C−1.8°C at the end of the 21st century. Under the medium- and high-emission scenarios (SSP4-3.4, SSP2-4.5, SSP4-6.0, SSP3-7.0, and SSP5-8.5), the annual mean temperature is expected to rise continuously at a rate of approximately 0.2°C/10yr−0.6°C/10yr (Fig. 7(a)). In the medium-term together with long-term periods, with increasing emissions, the annual mean temperature will gradually increase, with projected values of 1.6°C−2.9°C and 1.4°C−5.5°C, respectively. At the end of the 21st century, the temperature increase will be more apparent under higher emissions (Fig. 7(a1)).

In terms of annual precipitation, the growth rate is projected to be 1.8−12.3 mm/10yr under the various emission scenarios in the 21st century. Under the SSP1-2.6 and SSP1-1.9 (low-emission scenarios), the increase in precipitation will reach a maximum in the mid-term period (11.2% and 16.2%, apart respectively, relative to the 1995–2014 period) and then slow down. Under the medium- and high-emission scenarios (SSP5-8.5, SSP3-7.0, SSP4-6.0, SSP2-4.5, and SSP4-3.4), precipitation will continuously increase by the end of the 21st century (Fig. 7(b)). In the near and middle of the 21st century, the increase in annual precipitation will slow down as increases in radiative forcing, except in SSP5-8.5, with increasing precipitation rates of 6.5%−10.4% and 10.5%−16.2%, respectively, in the UYR relative to the reference period. Until the end of the 21st century, the increase of annual precipitation will naturally enhance with the increasing radiative forcing, with increases of 10.2%−28.5% under all seven scenarios. Annual precipitation increments vary greatly between different radiative forcing (Fig. 7(b1)). In addition, during all three study periods, the increase in precipitation in winter is the greatest under all SSPs.

4.2.2 Seasonal temperature and precipitation

Under all SSPs, seasonal temperature and precipitation have a significant upward trend in the 21st century over the UYR ($\alpha < 0.1$). Projections show that temperature in spring will continue to rise throughout the 21st century, while in other seasons, the temperature is expected to reach the highest in the middle of the 21st century and then slow down under lower-emission scenarios. Under other SSPs, seasonal temperatures will continue to rise. The projections also show that precipitation in spring and autumn will continue to increase under all SSPs, while precipitation in summer and winter will increase the most in the middle of the 21st century and then slow down under SSP1-1.9 and SSP1-2.6 but will continually

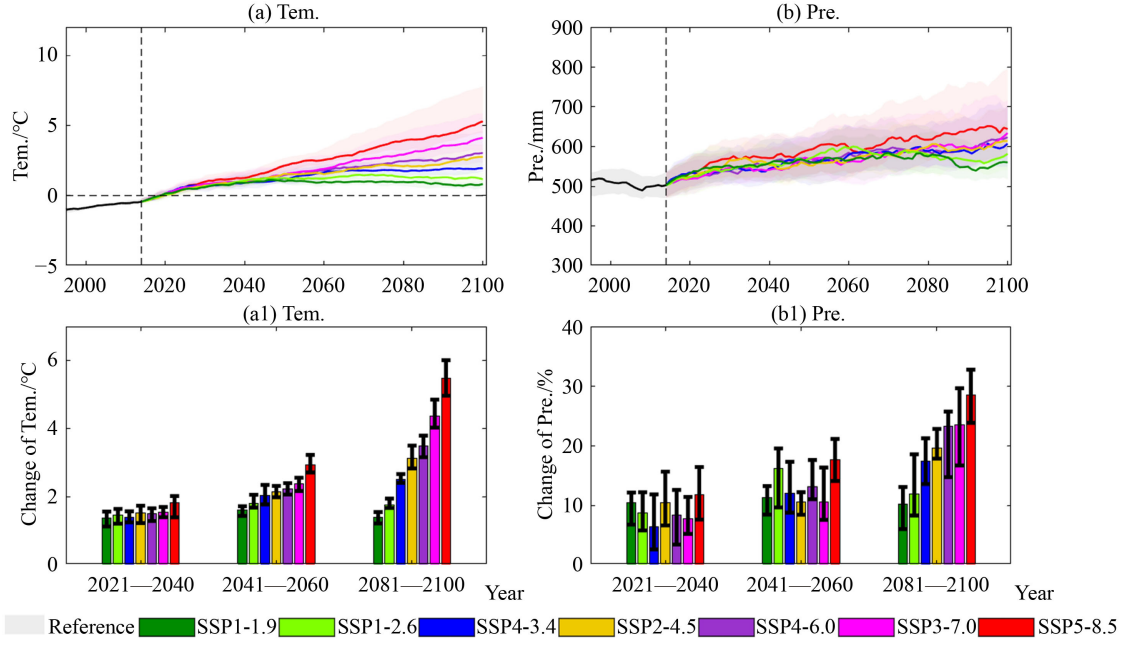

Fig. 7 The variations in annual precipitation and temperature for 2015−2100 in China's Upper Yellow River basin under the SSPs scenarios. Notes: shadow ranges represent the upper and lower quartile ranges of multiple models, and the lengths of black vertical lines indicate the same.

increase under other SSPs by the end of the 21st century.

Relative to the 1995−2014 period, in the near future, the seasonal temperature fluctuates with increasing radiative forcing. The temperature increase is the largest in autumn, with an increase of 1.4°C−2.2°C under SSP5-8.5, SSP3-7.0, SSP1-2.6, and SSP1-1.9. Under other scenarios, the temperature increase is the highest in spring at approximately 1.8°C. In the middle together with long-term of the 21st century, the temperature increase is the highest in autumn, i.e., approximately 1.8°C−3.2°C and 1.5°C−5.7°C (Figs. 8(a)−(d)).

Relative to the reference stage, except SSP5-8.5, summer precipitation enhancement will slow down with the increase in radiative forcing, increasing by 3.2%−6.2% and 3.3%−8.3% in the near- and mid-term, respectively, while precipitation increases in other seasons will fluctuate with the increase in radiative forcing. In the long term stage, the increasing summer precipitation is relatively less under low and high radiative forcings and is the greatest under medium radiative forcing. However, the precipitation increase in other seasons is greater with increasing radiative forcing (Figs. 8(a1)−(d1)).

4.3 Changes in river discharge under SSPs

4.3.1 Annual discharge

Based on the performance of HMs, different weights are assigned to each HM to obtain a multimodel-weighted ensemble. Figure 9 shows that under all seven SSPs, the annual discharge will significantly increase during the 21st century over the UYR ($\alpha < 0.01$). Under SSP1-2.6 and SSP1-1.9, the annual discharge will peak in the mid-term with maxima of 1130.0 m^3/s and 1162.6 m^3/s, and will slow and stabilize at 1097.0 and 1123.7 m^3/s in the long-term. Under SSP2-4.5, the increase in discharge during the near- to mid-term period will slow down but will continue to rise later and reach 1236.9 m^3/s by the end of the 21st century. Under other scenarios, the annual average discharge will rise continuously in all three periods and reach 1203.3, 1242.4, 1331.2, and 1482.1 m^3/s by the end of the 21st century (Fig. 9(a)).

To quantitatively reflect the changes in discharge in the next three periods under the SSPs, we analyzed the percentage change in discharge compared with a reference stage (Fig. 9(b)). In the near term, the annual mean discharge growth rate difference between high and low radiative forcings is small in the UYR, with an increase of 9%−20% relative to the reference stage. In addition to SSP5-8.5, the higher the radiative forcing, the smaller the discharge growth. The mid-term period features an increase of 10.2%−27.9% relative to the reference stage. Except for SSP5-8.5, the maximum emission scenario, the higher the radiative forcing is, the smaller the discharge increase. In the long-term, the projected increase is 15.2%−64.5%, but under different scenarios, the change in discharge growth is different from that in the previous two periods (Fig. 9(b)). The higher the radiative forcing is, the greater the discharge increase, and the difference in discharge significantly increases between different emission scenarios over time.

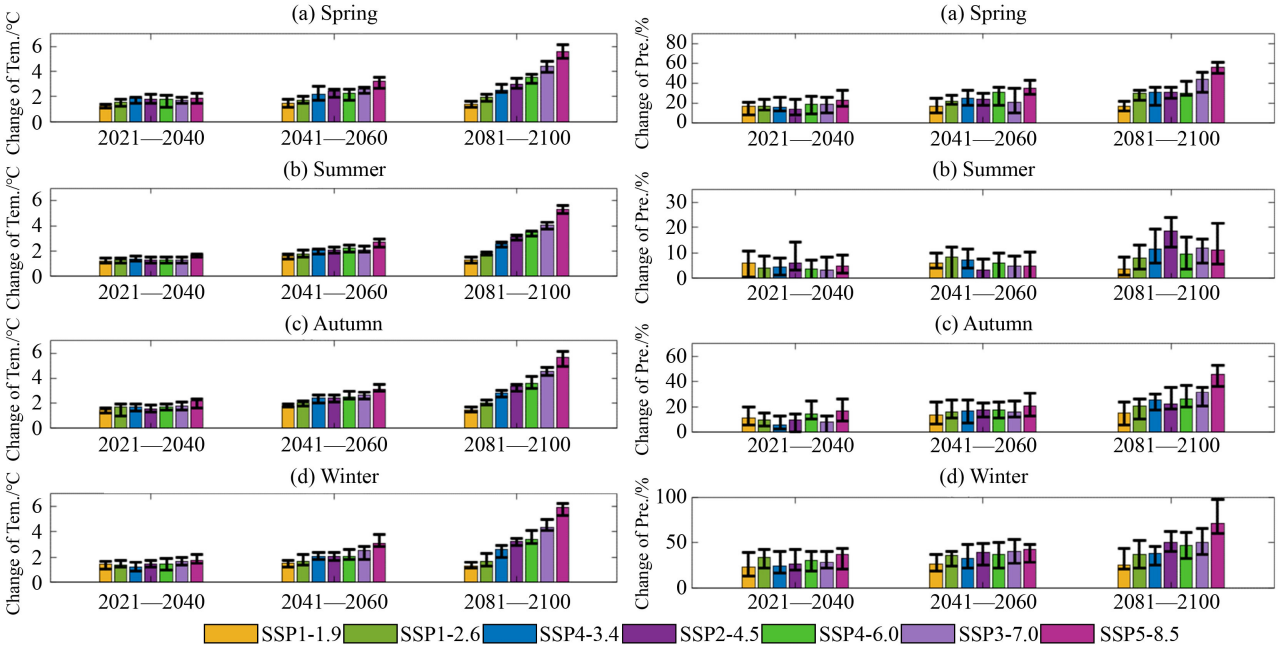

Fig. 8 The changes in near-, mid-, and long-term seasonal temperature (left) and precipitation (right) in the Upper Yellow River Basin under SSPs relative to 1995−2014 (i.e., 2021−2040, 2041−2060, and 2081−2100). Notes: the lengths of black vertical lines represent the upper and lower quartile range of multiple models.

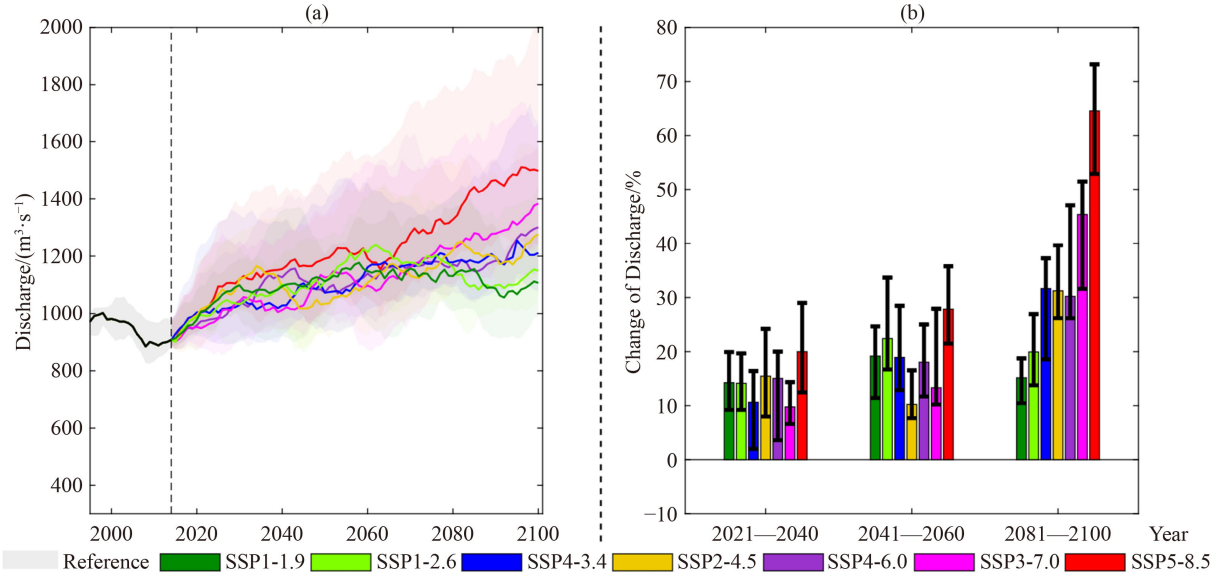

Fig. 9 Annual mean discharge under SSPs in the Upper Yellow River basin in China from 2015 to 2100. Notes: shadow ranges represent the upper and lower quartile ranges of multiple models, and the lengths of black vertical lines indicate the same.

The change in discharge growth in the three periods is highly similar to that of the annual precipitation increase in the same period.

4.3.2 Seasonal discharge

Under all the SSPs in the 21st century, seasonal discharge in the UYR has a significant upward trend. According to SSP4-6.0, SSP2-4.5, SSP4-3.4, SSP1-2.6 and SSP1-1.9, the maximum discharge increase is expected to be in spring and will increase by the end of the 21st century; under SSP5-8.5, and SSP3-7.0, the increasing seasonal discharge will be the largest in spring in the near and middle term of the 21st century but will change to autumn until the end of the 21st century (Fig. 10).

The observed discharge in summer and autumn in the UYR from 1961 to 2007 accounted for approximately 67% of the annual discharge, so the change in discharge in these two seasons was analyzed specifically. Figures 10(a1)−(b1) shows the percentage change in summer and autumn discharge in the UYR compared with the reference stage. In the near- and mid-term periods, except for SSP5-8.5, the increase in summer discharge will fluctuate and slow down, increasing by 6.4%−17.4% and 11.5%−18.4%, respectively, with increasing radiative forcing. However, in the long-term, the discharge will

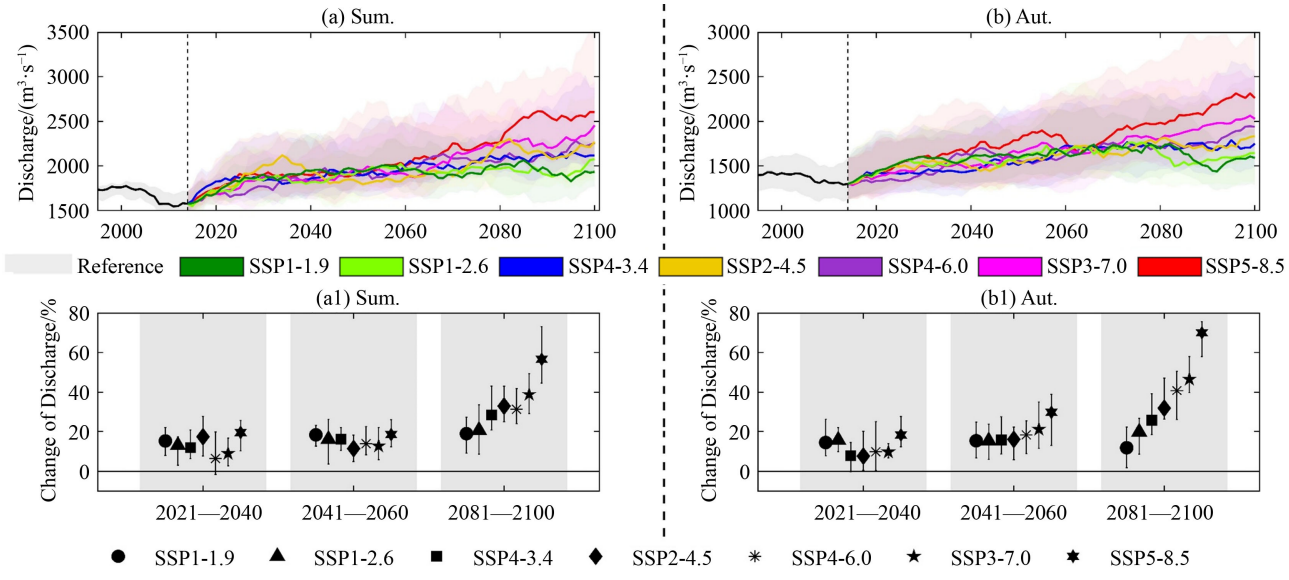

Fig. 10 Compared with the reference stage (from 1995 to 2014), the changes in summer discharge and autumn discharge in the Upper Yellow River basin under seven SSPs in the near, middle, and late 21st century. Notes: shadow ranges represent the upper and lower quartile ranges of multiple models, and the lengths of black vertical lines indicate the same.

continue to increase with increasing radiative forcing, rising by 18.9%−56.6%. For the amplification of autumn discharge, with the exception of SSP5-8.5, it will move toward mitigation in the near term, and yet in the medium term, discharge will increase slowly with the increase in radiative forcing, increasing by 12.8%−18.5% vs. base period. Discharge in the long-term is to be projected to increase continuously with increasing radiative forcing, which will reach 11.8%−70% under the SSPs.

The annual discharge in the UYR is expected to increase significantly during the 21st century, which has great implications for mitigating water shortages in the UYR.

4.3.3 Discharge extremes

The variation in quantile discharge over the UYR under the SSPs in the next three stages compared with the reference period is revealed in Fig. 11. This figure shows that in the 21st century, high flow (Q10) of UYR is expected to increase, and thus, the possibility of flooding in the UYR might increase. In the near term, the increase in Q10 is between 9.4% and 19.9%. The change in the extreme value of Q10 in different scenarios is similar to the annual precipitation change in the same stage, and the differences are small. In the mid-term, Q10 increases with fluctuations of 12.3%−24.7% under all SSPs. In addition, under SSP5-8.5, the increase in Q10 slows with increasing radiative forcing. Note that the possibility of flooding in the lowest emissions will be the highest. In the long-term, the Q10 value increases continuously from low- to high-emission scenarios and reaches the greatest increase of 53.4% under SSP5-8.5 (Fig. 11(a)).

Under SSP5-8.5, SSP4-6.0, SSP2-4.5, and SSP1-2.6, the Q90 value is higher than that in the reference period in all three future periods, indicating that the drought risk in the UYR might be reduced. However, Q90 will decrease by 5.9% and 0.8% under SSP4-3.4 and SSP3-7.0, respectively, in the near future and will decrease by 1.3% and 5%, respectively, under the SSP1-1.9 and SSP3-7.0 scenarios in the mid-term. These results indicate that there is the possibility that the drought risk in the UYR will increase.

5 Discussion

Previous studies in the UYR found that relative to 1971−2010, the annual mean temperature is expected to warm by 1°C−1.6°C in the mid-term and annual precipitation is expected to increase by 4.3%−5.7% in the same period under RCPs. Moreover, annual mean temperature and annual precipitation will increase by 2.1°C−3.8°C and 6%−8%, respectively compared with that in 1971−2000 in the long term (Kang et al., 2015; Wei et al., 2016; Chen, 2017). The current study shows

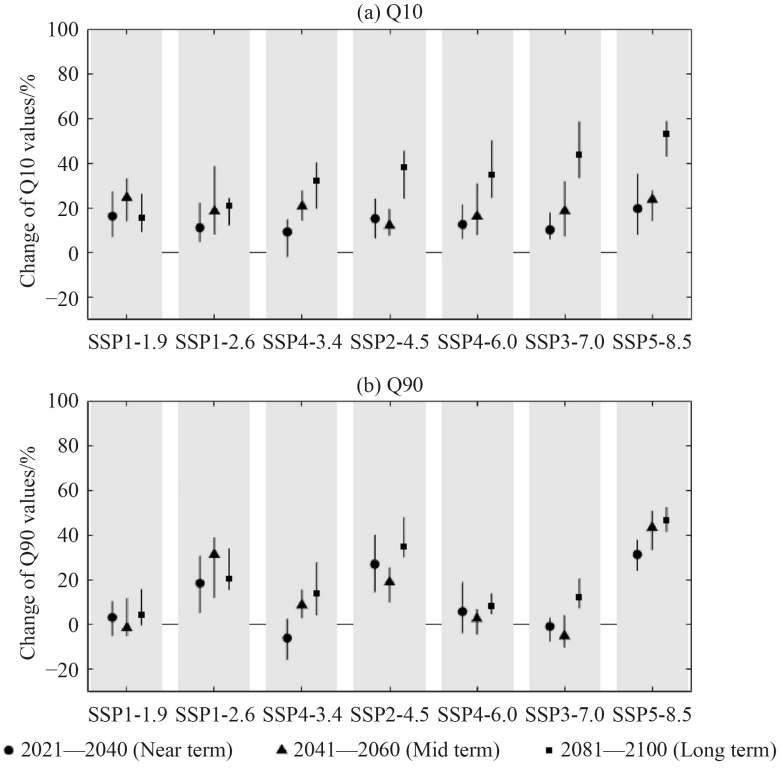

Fig. 11 The change of percentage in low flow (Q90) and high flow (Q10) for the near-, mid-, and long-term periods in China's Upper Yellow River basin under 7 SSPs scenarios (relative to the reference period, from 1995 to 2014). Notes: the lengths of black vertical lines represent the upper and lower quartile ranges of multiple models.

that relative to baseline period 1995−2014, the annual mean temperature is projected to increase by 1.6°C−2.9°C and 1.4°C−5.5°C in the mid-term and long-term periods, respectively, and annual precipitation will increase by 10.5%−16.2% and 10.2%−28.5% in the mid-term and long-term, respectively, under SSPs. Both of annual mean temperature and annual precipitation are significantly higher than the results of existing studies under RCPs.

In terms of streamflow, previous studies projected an increase of the annual discharge by 2.6%−8.1% in the mid-term but decrease by 2%−5% in the long term under RCPs, relative to 1971−2000 (Kang et al., 2015; Wei et al., 2016; Chen, 2017). Under SSPs, a persistent increase of annual mean discharge by10.2%−27.9% and 15.2%−64.5% is projected in the mid-term and long-term, respectively, relative to 1995−2014.

The differences in relative changes in future temperature, precipitation, and discharge exist due to the selection of the different reference periods, GCMs, and climate scenarios (Wei et al., 2016; Wang et al., 2020). The current study analyzes future hydro-climate trends in the three time periods based on the CMIP6 updated climate models and scenarios. To distinguish the effects of different radiative forcings, CMIP5 requires that the differences between radiative forcings in different RCPs are large enough in 2100 (Vuuren et al., 2011), which inevitably ignores the influence of small differences in radiative forcing levels on the trend and amplitude of factor changes (Zhang et al., 2019). The CMIP6 experiment maintains four classical CMIP5 emission paths, and simultaneously, adds three more emission scenarios, SSP3-7.0, SSP4-3.4, and SSP1-1.9. The smaller global average radiative forcing difference makes the research results more refined and compensates for the radiative forcing gap of the CMIP5. It is worth noting that in the near- and mid-term, except for SSP5-8.5, increasing scope in annual precipitation and discharge in the UYR relative to the reference stage will be reduced under the low to the high radiative forcing scenarios.

6 Conclusions

In this paper, five GCMs from CMIP6 were bias-corrected and downscaled to study the climate change and discharge change in the UYR under 7 SSPs (namely, SSP1-1.9, SSP1-2.6, SSP2-4.5, SSP3-7.0, SSP4-3.4, SSP4-6.0, and SSP5-8.5). Three HMs (SWAT, HBV-D, and VIC) driven by the GCMs are used to simulate discharge at the Lan Zhou, Tang Naihai, Ma Qu, and Ji Mai hydrological stations in the UYR from 1995 to 2100 based on parameters calibrated and validated in historical periods. This paper comprehensively evaluates the applicability of HMs to ensure the reliability of hydrological simulations. The changes in temperature, precipitation, and annual, seasonal, and daily discharge extremes in the UYR under the seven SSPs in three future periods are summarized as follows.

1) Under the SSPs, the UYR will experience significantly warmer and wetter conditions in the 21st century. Seasonal temperature and precipitation over the UYR will have a significant upward trend during the 21st century. The largest temperature increase in the three future periods will be mostly in autumn. Most seasonal precipitation will increase with the increase of radiative forcing throughout the 21st century except summer precipitation which decreases with the increase of radiative forcing in the near- and mid-term.

2) Annual discharge is projected to increase significantly ($\alpha < 0.01$) during the 21st century over the UYR. Under all SSPs, in the three future periods, the maximum increase in discharge is expected to occur in spring mostly. In the near- and mid-term periods, except under SSP5-8.5, the increased rates of annual discharge and summer discharge will slow down with the increase of radiative forcing. In the long-term, summer discharge will be highest under SSP2-4.5, but the increase in annual and other seasonal discharge will accelerate with the increase of radiative forcing.

3) Flood risk will increase over the UYR during the entire 21st century. Relative to the reference stage, the drought risk in the 21st century will be reduced under the four upgraded CMIP5 scenarios. Under the three new scenarios, there are situations where the risk of drought might increase in the near- and mid-term periods.

It is essential to note that impacts of climate change on streamflow in this paper are investigated under the assumption that the optimal parameters calibrated/validated in the historical period remain valid in the future. Besides, climate models, the parameterization process of hydrological models, and human interferences on river regime all introduce uncertainties that affect the research results. Although multiple climate and hydrological models and new scenarios applied in the current study can improve the projection of hydro-climatic conditions in future to a certain extent, there are still large uncertainties. In next step, more reliable climate models, more effective parametric schemes for HMs, and more consideration for human activities are needed to reduce the uncertainty of projection.

The current study deepens the research on discharge simulation and projection in the UYR in the context of climate change and can be used as a reference study for various basins with similar climatic and hydrological conditions to calibrate and verify HMs and assign weight to each model.

Acknowledgments This study was jointly supported by the International Cooperation Program between the National Science Foundation of China (NSFC) and United Nations Environment Program (UNEP) (Grant No. 42261144002), and the Jiangxi Meteorological Bureau (No. JX201810) and

the High-level Talent Recruitment Program of the Nanjing University of Information Science and Technology.

Competing interests The authors declare that they have no competing interests.

References

Arnold J, Srinivasan R, Muttiah R, Williams J R (1998). Large area hydrologic modeling and assessment part I: model development. J Am Water Resour Assoc, 34(1): 73–89

Arsenault R, Gatien P, Renaud B, Brissette F, Martel J (2015). A comparative analysis of 9 multimodel averaging approaches in hydrological continuous streamflow simulation. J Hydrol (Amst), 529: 754–767

Bergström S, Forsman A (1973). Development of a conceptual deterministic rainfall-runoff model. Nord Hydrol, 4(3): 147–170

Chang J, Wei J, Wang Y, Yuan M, Guo J (2017). Precipitation and runoff variations in the Yellow River Basin of China. J Hydroinform, 19(1): 138–155

Chen L (2017). Responses of water resources to the climate change in the Yellow River Basin. Dissertation for Master's Degree. Xi'an: Xi'an University of Technology (in Chinese)

Chen Z, Wang Y, Su B, Huang J, Jiang T (2020). Research on the response of runoff to climate change in Wujiang River Basin based on multi-model (1861–2018). Resources and Environment in the Yangtze Basin, 30(08): 1927–1937 (in Chinese)

Dawson C W, Mount N J, Abrahart R J, Shamseldin A Y (2012). Ideal point error for model assessment in data-driven river flow forecasting. Hydrol Earth Syst Sci, 16(8): 3049–3060

Eghdamirad S, Johnson F, Sharma A, Kim J H (2019). The influence of dependence in characterizing multivariable uncertainty for climate change impact assessments. Hydrol Sci J, 64(6): 731–738

Franke R (1982). Scattered data interpolation: tests of some methods. Math Comput, 38(157): 181–200

Gao C, Su B, Krysanova V, Zha Q, Chen C, Luo G, Zeng X, Huang J, Xiong M, Zhang L, Jiang T (2019). A 439-year daily discharge dataset (1861–2299) for the upper Yangtze River, China. Earth System Science Data Discussions, 1–26

Gidden M J, Riahi K, Smith S J, Fujimori S, Luderer G, Kriegler E, van Vuuren D P, van den Berg M, Feng L, Klein D, Calvin K, Doelman J C, Frank S, Fricko O, Harmsen M, Hasegawa T, Havlik P, Hilaire J, Hoesly R, Horing J, Popp A, Stehfest E, Takahashi K (2019). Global emissions pathways under different socioeconomic scenarios for use in CMIP6: a dataset of harmonized emissions trajectories through the end of the century. Geosci Model Dev, 12(4): 1443–1475

Gupta H V, Kling H, Yilmaz K K, Martinez G F (2009). Decomposition of the mean squared error and NSE performance criteria: implications for improving hydrological modelling. J Hydrol, 377(1−2): 80–91

Hamed R, Ramachandra Rao A (1998). A modified Mann-Kendall trend test for autocorrelated data. J Hydrol (Amst), 204(1): 182–196

Hausfather Z, Peters G P (2020). Emissions – the 'business as usual' story is misleading. Nature, 577(7792): 618–620

Höllermann B, Evers M (2017). Perception and handling of uncertainties in water management—a study of practitioners' and scientists' perspectives on uncertainty in their daily decision-making. Environ Sci Policy, 71: 9–18

Huang J (2014). Study on Changes of Runoff in Cuntan Catchment of the Yangtze river. Dissertation for Master's Degree. Nanjing: Nanjing University of Information Science & Technology (in Chinese)

Huang J, Zhai J, Jiang T, Wang Y, Li X, Wang R, Xiong M, Su B, Fischer T (2018). Analysis of future drought characteristics in China using the regional climate model CCLM. Clim Dyn, 50(1): 507–525

IPCC (2001).Climate Change 2001: The Scientific Basis. In: Contribution of Working Group I to the Third Assessment Report of the Intergovernmental Panel on Climate Change. Cambridge: Cambridge University Press

IPCC (2021). Climate Change 2021: The Physical Science Basis. In: Contribution of Working Group I to the Fifth Assessment Report of the Intergovernmental Panel on Climate Change. Cambridge: Cambridge University Press

Jia Y, Dong Z, Bian J, Zhong D, Lin M (2019). Research on multi-objective optimal operation of the cascade reservoirs of the Upper Yellow River. Yellow River, 41(1): 41–45, 50 (in Chinese)

Kang L, Ruby L L, Liu C, Wang S (2015). Simulative study of future climate and hydrological change over the Yellow River basin. Acta Meteorol Sin, 73(2): 382–393 (in Chinese)

Krysanova V, Bronstert A, Müller-Wohlfeil D I (1999). Modelling river discharge for large drainage basins: from lumped to distributed approach. Hydrol Sci J, 44(2): 313–331

Krysanova V, Donnelly C, Gelfan A, Gerten D, Arheimer B, Hattermann F, Kundzewicz Z W (2018). How the performance of hydrological models relates to credibility of projections under climate change. Hydrol Sci J Hydrologiques, 1–25

Lambert S J, Boer G J (2001). CMIP1 evaluation and intercomparison of coupled climate models. Clim Dyn, 17(2−3): 83–106

Li C, Jiang T, Wang Y, Miao L, Li S, Chen Z, Lv Y (2022). Simulation and estimation of future air temperature in upper basin of the Yellow River based on CMIP6 models. J Glaciol Geocryol, 44(01): 171–178 (in Chinese)

Li H, Sheffield J, Wood E F (2010). Bias correction of monthly precipitation and temperature fields from Intergovernmental Panel on Climate Change AR4 models using equidistant quantile matching. J Geophys Res, 115: D10101

Liang X, Lettenmaier D P, Wood E F, Burges S (1994). A simple hydrologically based model of land surface water and energy fluxes for general circulation models. J Geophys Res, 99(D7): 14415–14428

Mann H B (1945). Nonparametric tests against trend. Econometrica, 13(3): 245–259

Meng F, Su F, Yang D, Tong K, Hao Z (2016). Impacts of recent climate change on the hydrology in the source region of the Yellow River basin. J Hydrol (Amst), 6(C): 66–81

Moran P A P, Kendall M G (1951). Rank correlation methods. J R Stat Soc (Ser A), 114(1): 99–100

Moriasi D N, Arnold J G, Van Liew M W, Bingner R L, Harmel, R D,

Veith T L (2007). Model evaluation guidelines for systematic quantification of accuracy in watershed simulations. Transactions of the ASABE, 50(3): 885–900

O'Neill B C, Tebaldi C, van Vuuren D P, Eyring V, Friedlingstein P, Hurtt G, Knutti R, Kriegler E, Lamarque J F, Lowe J, Meehl G A, Moss R, Riahi K, Sanderson B M (2016). The scenario model intercomparison project (ScenarioMIP) for CMIP6. Geosci Model Dev, 9(9): 3461–3482

Peng S, Shang W, Wang Y, Jun L, Zheng X (2018). Research on ecological impacts of the joint operation of cascade reservoirs in the upstream of the Yellow River. J Hydraul Eng (NYNY), 49: 1187–1198

Puertes C, Lidón A, Echeverría C, Bautista I, González-Sanchis M, del Campo A D, Francés F (2019). Explaining the hydrological behaviour of facultative phreatophytes using a multi-variable and multi-objective modelling approach. J Hydrol (Amst), 575: 395–407

Qin J, Su B, Tao H, Wang Y, Huang J, Jiang T (2021). Projection of temperature and precipitation under SSPs-RCPs Scenarios over northwest China. Front Earth Sci, 15(1): 23–37

Qin P, Liu M, Du L, Xu H, Liu L, Xiao C (2019). Climate change impacts on runoff in the upper Yangtze River basin. Climate Change Research, 15(4): 405–415 (in Chinese)

Ritter A, Muñoz-Carpena R (2013). Performance evaluation of hydrological models: statistical significance for reducing subjectivity in goodness-of-fit assessments. J Hydrol, 480: 33–45

Shamseldin A Y, O'connor K M, Nasr A E (2007). A comparative study of three neural network forecast combination methods for simulated river flows of different rainfall—runoff models. Hydrol Sci J, 52(5): 896–916

Stocker T, Qin D, Plattner G (2014). Climate change 2013: the physical science basis. In: Contribution of working group into the fifth assessment report of IPCC the intergovernmental panel on climate change, 18(2): 95–123

Su B, Huang J, Zeng X, Gao C, Jiang T (2017). Impacts of climate change on streamflow in the upper Yangtze River basin. Clim Change, 141(3): 533–546

Sun Y (2021). Impact of human activities on climate system: an interpretation of Chapter I of WGI report of IPCC AR6. Transact Atmosph Sci, 44(5): 654–657 (in Chinese)

Taylor K E (2001). Summarizing multiple aspects of model performance in a single diagram. J Geophys Res, 106(D7): 7183–7192

Taylor K E, Stouffer R J, Meehl G A (2012). An overview of CMIP5 and the experiment design. Bull Am Meteorol Soc, 93(4): 485–498

Torres R R, Marengo J A (2014). Climate change hotspots over South America: from CMIP3 to CMIP5 multi-model datasets. Theor Appl Climatol, 117(3−4): 579–587

van Vuuren D P, Edmonds J, Kainuma M, Riahi K, Thomson A, Hibbard K, Hurtt G C, Kram T, Krey V, Lamarque J F, Masui T, Meinshausen M, Nakicenovic N, Smith S J, Rose S K (2011). The representative concentration pathways: an overview. Clim Change, 109(1−2): 5–31

Vetter T, Huang S, Aich V, Yang T, Wang X, Krysanova V, Hattermann F (2015). Multi-model climate impact assessment and intercomparison for three large-scale river basins on three continents. Earth Syst Dyn, 6(1): 17–43

Wang G, Qiao C, Liu M, Du F, Ye T, Wang J (2020). The future water resources regime of the Yellow River basin in the context of climate change. Hydro-Sci Engineer, 180(2): 4–11 (Chinese)

Wang L, Li Y, Qixiang C, Wu S, Fang F (2016). A new method of multi model ensemble to improve the simulation of the geographic distribution of Köppen-Geiger climate classification. AGU Fall Meeting Abstracts

Wang Y, Quan Q, Xue T, Shen B, Zhang X (2018). Hydrological impact of climate change on the source region of the Yellow River. J Water Resourc Res, 7(2): 135–143

Wei J, Chang J, Chen L (2016). Runoff change in upper reach of Yellow River under future climate change based on VIC model. J Hydroelectric Engineer, 35(05): 65–74 (in Chinese)

Wei Y, Li X, Li F (2021). Spatial distribution characteristics and influencing factors of wet and dry of runoff in the upper reaches of the Yellow River. Water Resourc Protect, 37(06): 103–113 (in Chinese)

Wen S, Su B, Wang Y, Zhai J, Sun H, Chen Z, Huang L, Wang A, Jiang T (2020). Comprehensive evaluation of hydrological models for climate change impact assessment in the Upper Yangtze River Basin, China. Clim Change, 163(3): 1207–1226

Xi J, Yang X, Lv X, Hu H (2021). Hydrological simulation of Heihe and Baihe River Basin based on SWAT model. Yellow River, (10): 60–66+113 (in Chinese)

Yan Y (2017). Simulation of water resources in the upper reaches of the Yellow River and its future evolution. Dissertation for Master's Degree. Shanghai: East China Normal University (in Chinese)

Zhang L, Chen X, Xin X (2019). Short commentary on CMIP6 Scenario Model Intercomparison Project (ScenarioMIP). Climate Change Res, 15(05): 519–525 (in Chinese)

Zhao M, Su B, Wang Y, Wang A, Jiang T (2020). Impacts of climate change on river runoff at the Ganjiang and Guanting River basins in the eastern monsoon region. Climate Change Res, 16(6): 679–689 (in Chinese)

Zhou T, Zou L, Chen X (2019). Commentary on the coupled model intercomparison project phase 6 (CMIP6). Climate Change Res, 15(5): 445–456 (in Chinese)

Zuo Q (2019). Research framework for ecological protection and high-quality development in the Yellow River Basin. Yellow River, 41(11): 1–6+16 (in Chinese)